

A step to the decentralized real-time timekeeping network

Fangmin Wang(王芳敏), Yufeng Chen(陈雨锋), Jianhua Zhou(周建华), Yuting Lin(蔺玉亭), Jun Yang(杨军), Bo Wang(王波), and Lijun Wang(王力军)
Citation: Chin. Phys. B, 2024, 33 (**1**): 010702. DOI: 10.1088/1674-1056/acfa88
Journal homepage: http://cpb.iphy.ac.cn; http://iopscience.iop.org/cpb

What follows is a list of articles you may be interested in

A combined magnetic field stabilization system for improving the stability of $^{40}Ca^{+}$ optical clock

Mengyan Zeng(曾孟彦), Zixiao Ma(马子晓), Ruming Hu(胡如明), Baolin Zhang(张宝林), Yanmei Hao(郝艳梅), Huaqing Zhang(张华青), Yao Huang(黄垚), Hua Guan(管桦), and Kelin Gao(高克林)
Chin. Phys. B, 2023, 32 (**11**): 110704. DOI: 10.1088/1674-1056/acf5d5

Optical state selection process with optical pumping in a cesium atomic fountain clock

Lei Han(韩蕾), Fang Fang(房芳), Wei-Liang Chen(陈伟亮), Kun Liu(刘昆), Ya-Ni Zuo(左娅妮), Fa-Song Zheng(郑发松), Shao-Yang Dai(戴少阳), and Tian-Chu Li(李天初)
Chin. Phys. B, 2021, 30 (**8**): 080602. DOI: 10.1088/1674-1056/ac0698

A 532 nm molecular iodine optical frequency standard based on modulation transfer spectroscopy

Feihu Cheng(程飞虎), Ning Jin(金宁), Fenglei Zhang(张风雷), Hui Li(李慧), Yuanbo Du(杜远博), Jie Zhang(张洁), Ke Deng(邓科), and Zehuang Lu(陆泽晃)
Chin. Phys. B, 2021, 30 (**5**): 050603. DOI: 10.1088/1674-1056/abd754

Development of the integrated integrating sphere cold atom clock

Ming-Yuan Yu(于明圆), Yan-Ling Meng(孟艳玲), Mei-Feng Ye(叶美凤), Xin Wang(王鑫), Xin-Chuan Ouyang(欧阳鑫川), Jin-Yin Wan(万金银), Ling Xiao(肖玲), Hua-Dong Cheng(成华东), Liang Liu(刘亮)
Chin. Phys. B, 2019, 28 (**7**): 070602. DOI: 10.1088/1674-1056/28/7/070602

Fiber-based multiple-access frequency synchronization via 1f-2f dissemination

Xi Zhu(朱玺), Bo Wang(王波), Chao Gao(高超), Li-Jun Wang(王力军)
Chin. Phys. B, 2016, 25 (**9**): 090601. DOI: 10.1088/1674-1056/25/9/090601

INSTRUMENTATION AND MEASUREMENT

A step to the decentralized real-time timekeeping network

Fangmin Wang(王芳敏)[1,2], Yufeng Chen(陈雨锋)[1,2], Jianhua Zhou(周建华)[3], Yuting Lin(蔺玉亭)[3], Jun Yang(杨军)[4], Bo Wang(王波)[1,2,†], and Lijun Wang(王力军)[1,2]

[1] *State Key Laboratory of Precision Space-time Information Sensing Technology, Department of Precision Instrument, Tsinghua University, Beijing* 100084, *China*

[2] *Key Laboratory of Photonic Control Technology (Ministry of Education), Tsinghua University, Beijing* 100084, *China*

[3] *Beijing Satellite Navigation Center, Beijing* 100094, *China*

[4] *Beijing Institute of Radio Metrology and Measurement, Beijing* 100854, *China*

(Received 19 July 2023; revised manuscript received 8 September 2023; accepted manuscript online 18 September 2023)

The composite time scale (CTS) provides an accurate and stable time-frequency reference for modern science and technology. Conventional CTS always features a centralized network topology, which means that the CTS is accompanied by a local master clock. This largely restricts the stability and reliability of the CTS. We simulate the restriction and analyze the influence of the master clock on the CTS. It proves that the CTS's long-term stability is also positively related to that of the master clock, until the region dominated by the frequency drift of the H-maser (averaging time longer than $\sim 10^5$ s). Aiming at this restriction, a real-time clock network is utilized. Based on the network, a real-time CTS referenced by a stable remote master clock is achieved. The experiment comparing two real-time CTSs referenced by a local and a remote master clock respectively reveals that under open-loop steering, the stability of the CTS is improved by referencing to a remote and more stable master clock instead of a local and less stable master clock. In this way, with the help of the proposed scheme, the CTS can be referenced to the most stable master clock within the network in real time, no matter whether it is local or remote, making democratic polycentric timekeeping possible.

Keywords: frequency synchronization network, composite time scale, frequency stability, democratic timekeeping

PACS: 06.30.Ft, 06.20.–f

DOI: 10.1088/1674-1056/acfa88

1. Introduction

Time serves as the foundation of modern science and technology, including navigation and positioning,[1] telecommunication systems,[2] geodesy,[3] smart electricity grids,[4] gravitational wave detection,[5] and hunting for dark matter.[6] To maintain an accurate, stable and uniform time in a certain district, the atomic time scale is widely adopted in timekeeping institutes worldwide. It can be generated based on either a single atomic clock or an ensemble of atomic clocks (also named as composite time scale, CTS, whose basic idea is shown in Fig. 1).[7] Compared with the former, the CTS has obvious advantages in stability and reliability.[7,8] Various atomic clocks, together with an efficient ensemble algorithm, can effectively reduce the output noise of the CTS. Consequently, many standalone atomic time scales employ the CTS method.[9–15]

According to two features (the clock ensemble is distributed or co-located, and the CTS is generated in real time or in deferred time), the CTS can be classified into four types: distributed real-time CTS, distributed deferred CTS, co-located real-time CTS, and co-located deferred CTS. Among them, co-located CTS is most extensively applied by timekeeping institutes. Nevertheless, the main station where the clock ensemble located may be destroyed by earthquakes, fires, or other uncontrollable factors, leading to the outage of the co-located CTS. On the other hand, the performance of CTS is also adversely affected by environment-induced correlation among co-located clocks. To overcome these problems, distributed CTS has been studied and applied. For example, we have realized a real-time CTS based on the distributed clocks scattered around the Beijing region.[16] More typical CTS is generated with a clock ensemble containing both co-located and remote atomic clocks that always form a clock network, such as TA (PL).[17,18] However, all these CTSs still share a common shortcoming, i.e., centralized timekeeping topology, which is manifested in two aspects. From the perspective of a timekeeping institution within the clock network, the most stable clock within the local ensemble is always chosen as the master clock to generate the CTS. This will lead to the following problems. First, the local master clock may have failed or deteriorated in some cases, which will result in deterioration of the physical realization of CTS (denoted as physical CTS) or even interruption of its output. Second, the local master clock is not always the most stable atomic clock in the whole network, preventing further improvements in the stability and reliability of the physical CTS. From the perspective of the entire clock network, the best physical CTS can only be achieved at a timekeeping institution with the best clock on

†Corresponding author. E-mail: bo.wang@tsinghua.edu.cn

© 2024 Chinese Physical Society and IOP Publishing Ltd

account of the tight dependency of the physical CTS on the master clock.

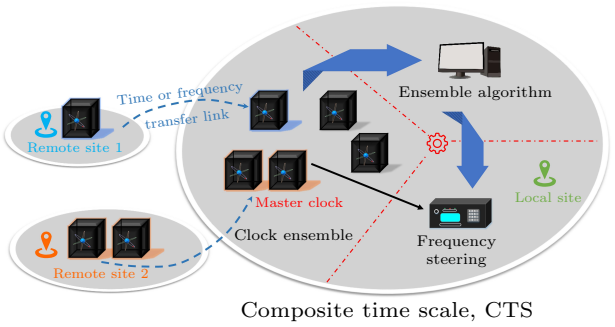


Fig. 1. Schematic diagram of CTS.

In this paper, we first simulate the stability limitation of the physical CTS caused by the selection of the master clock. Further analysis of the mechanism inherent in this limitation is presented. To break this limitation, a real-time clock network is utilized. Using four distributed clocks in the network, a real-time physical CTS referenced by a stable remote master clock is demonstrated. In comparison, based on the same clocks, another real-time physical CTS is generated by referencing to a less stable local master clock. They have been running continuously for more than 90 days, and their stability results are given. It shows that by employing a more stable remote master clock supported by the network, the performance evaluation index of the physical CTS, i.e., the averaging time when the CTS outperforms the member clocks, can be enhanced by a factor of two. In this way, the physical CTS can be realized with the most stable clock as the master clock in real time no matter whether it is local or remote. At the same time, the best physical CTS can be realized no matter whether the timekeeping institution has the most stable clock, thus making polycentric democratic timekeeping possible. This means that the scheme can break the limitation of centralized network topology on the physical CTS's stability.

The rest of this paper is organized as follows. The influence of the master clock on the physical CTS is simulated and the mechanism inherent in this influence is analyzed in Section 2. In Section 3, a real-time physical CTS referenced by a stable remote master clock is demonstrated based on a real-time clock network, indicating that the physical CTS can be realized in real time with the most stable clock as the master clock enabled by the network. We also take a comparison experiment to verify the strength experimentally in this section. Finally, Section 4 concludes this paper.

2. Simulating the influence of the master clock on the physical CTS

The physical CTS is usually achieved by periodically adjusting the output frequency of an auxiliary output generator (AOG) referenced by the master clock. The adjustment is carried out according to the paper CTS, which refers to the paper form of the CTS and is calculated from the phase time differences of the clock ensemble with the ensemble algorithm. It is widely accepted that the properties of physical CTS are determined by both the paper CTS and the master clock. Nevertheless, what extent does the master clock affect the stability of the physical CTS? What is the intrinsic mechanism of this judgment under open-loop steering? We have conducted a simulation to demonstrate this process and performed the corresponding theoretical analysis.

2.1. Simulation of an atomic clock ensemble and AOG noise floor

To analyze the influence of the master clock on the physical CTS, we simulate an atomic clock ensemble containing four H-masers at different levels of stability. In general, the typical phase time of an H-maser can be modeled as a quadratic polynomial combined with random noise.[7,19,20] Hence, the noise types and parameters of H-masers need to be determined first. By piecewise fitting the individual stability curve of the H-maser, the main noise types and the intensity of noise can be obtained for each H-maser.[21,22] For the four H-masers used in our experimental setup, the dominant noise is identified as white frequency modulation (WFM), white phase modulation (WPM), and flicker frequency modulation (FFM). Then, the H-maser model used here can be defined as

$$x_i(t) = x_i(0) + y_i(0)t + \frac{1}{2}d_i t^2 + \sigma_i^{\mathrm{I}}\varepsilon_i^{\mathrm{I}}(t) + \sigma_i^{\mathrm{II}}\varepsilon_i^{\mathrm{II}}(t) + \sigma_i^{\mathrm{III}}\varepsilon_i^{\mathrm{III}}(t),$$
$$i = \mathrm{A},\mathrm{B},\mathrm{C},\mathrm{D}, \tag{1}$$

where x_i and y_i represent the phase time and fractional frequency of the clock i with respect to an ideal clock, respectively; d_i is the frequency drift of the clock i with respect to an ideal clock; $\varepsilon_i^{\mathrm{I}}(t)$, $\varepsilon_i^{\mathrm{II}}(t)$ and $\varepsilon_i^{\mathrm{III}}(t)$ represent FFM, WFM and WPM, respectively; σ_i^{I}, σ_i^{II} and σ_i^{III} denote diffusion coefficients for the magnitude of these three types of noise.

We also simulate the noise floor of AOG with a similar method. The simulation parameters of the H-masers and AOG noise floor are listed in Table 1. Using these parameters, we generate the data of the H-maser ensemble and AOG noise floor spanning 20 days with a time interval of 1 s. Their stability curves are shown in Fig. 2(a), where clock C is the most stable clock, while clock D is the least stable clock.

2.2. Simulation of physical CTSs with different master clocks

Two physical CTSs referenced by clocks C and D are generated in the simulative method based on the simulated data. The generation process consists of two steps. The first step is to calculate the paper CTS, which is a sequence of phase time differences between the CTS and the master clock. The ensemble algorithm used in the step is AT1, and the weight

of each clock is determined by its performance with reference to the paper CTS.[23] It generates the paper CTS periodically and iteratively. The calculation interval is set to 1200 s. The second step is to simulate the physical CTS based on the selected master clock according to the corresponding paper CTS. Specifically, it is necessary to first convert the paper CTS into the frequency adjustment quantity. Then, the frequency adjustment quantity is added to the frequency of the AOG's reference signal, which is exactly the frequency of the master clock, during each adjustment interval. This operation is actually implemented by adding a linear accumulation of frequency adjustment quantity over time to the phase time of the master clock during each adjustment interval. The adjustment interval here is set to be equal to the calculation interval of paper CTS. After that, the AOG noise floor is superimposed on the phase time of the master clock.

Table 1. Simulative parameters of the clock ensemble and AOG noise floor.

Parameters	A	B	C	D	AOG noise floor
FFM diffusion coefficient σ_i^{I}	1.5×10^{-15}	1.5×10^{-15}	1×10^{-15}	2×10^{-15}	
WFM diffusion coefficient σ_i^{II}	8×10^{-14}	7×10^{-14}	5×10^{-14}	1×10^{-13}	1.5×10^{-14}
WPM diffusion coefficient σ_i^{III}	9×10^{-14}	8×10^{-14}	6×10^{-14}	1×10^{-13}	4×10^{-14}
Frequency offset $y_i(0)$	1×10^{-12}	1×10^{-13}	1×10^{-13}	7×10^{-13}	
Frequency drift d_i	5×10^{-22}	4×10^{-22}	3×10^{-22}	1×10^{-22}	

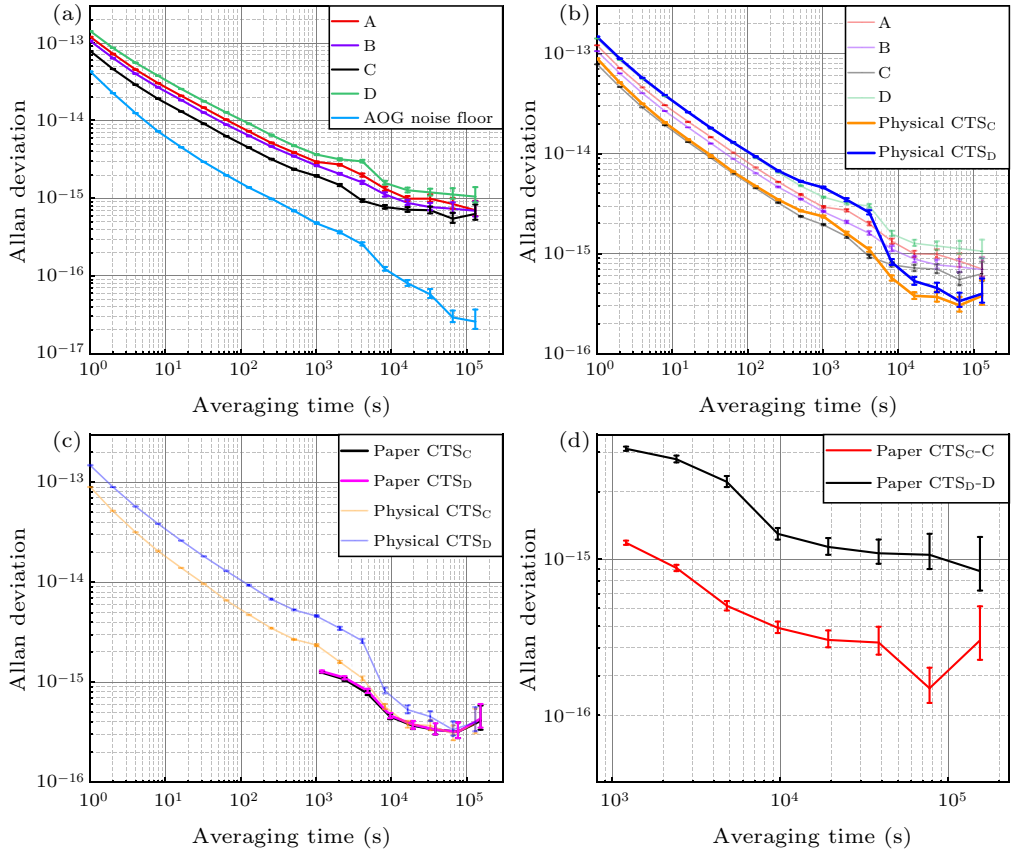


Fig. 2. Simulation results of physical CTSs with different master clocks. (a) Stability curves of simulated H-maser ensemble and AOG noise floor, where clock C is the most stable, while clock D is the least stable; A, B, C, and D: simulated H-masers; AOG: auxiliary output generator. (b) Individual stability curves of simulated physical CTSs referenced by clock C (the most stable clock) and clock D (the least stable clock), respectively, as well as that of member clocks. Physical $\mathrm{CTS_C}$ represents physical CTS referenced by clock C, other legends have similar meanings. (c) Individual stability curves of simulated physical CTSs referenced by clocks C and D, respectively, as well as that of the corresponding paper CTSs. Paper $\mathrm{CTS_C}$ represents paper CTS referenced by clock C, other legends have similar meanings. (d) Relative stability curves of paper CTSs with respect to clock C and clock D, respectively. Paper $\mathrm{CTS_C}$-C represents paper CTS referenced by clock C with respect to clock C, other legends have the similar meanings.

To evaluate the effect of master clock selection on the stability of physical CTS, the individual stabilities of physical CTSs referenced by different master clocks are obtained. The individual stabilities of paper CTSs are also calculated to assist in the analysis. The stability results are shown in Figs. 2(b) and 2(c).

It can be seen from Fig. 2(b) that the individual stabilities of physical CTSs referenced by different master clocks diverge obviously from each other. The physical CTS's "short-term stability when averaging time is shorter than the adjustment in-

terval" (SSSAI) almost follows that of the corresponding master clock. In regard to the "long-term stability when the averaging time is longer than the adjustment interval" (LSLAI), the physical CTS referenced by clock C (the most stable clock) outperforms all clocks when the averaging time is longer than ~ 5000 s, while the physical CTS referenced by clock D (the least stable clock) outperforms all clocks when the averaging time is longer than ~ 10000 s. It demonstrates that by employing a more stable master clock, the performance evaluation index of the physical CTS, i.e., the averaging time when the CTS outperforms the member clocks, can be enhanced by a factor of 2.

To investigate the mechanism inherent in this phenomenon, the individual stabilities of paper CTSs and physical CTSs are compared. It can be seen from Fig. 2(c) that the individual stabilities of the paper CTSs remain identical when clocks at different stability levels are used as references. When the averaging time is equal to the adjustment interval, 1200 s, the bias between the individual stability of paper CTS and that of physical CTS referenced by clock C is $\sim 1\times10^{-15}$, while the bias between the individual stability of paper CTS and that of physical CTS referenced by clock D is $\sim 3\times10^{-15}$. These quantities also reflect the magnitude of the frequency error introduced by frequency steering. Moreover, the stability of the physical CTS referenced by clock C is closer to that of paper CTS compared with that of physical CTS referenced by clock D.

The results will be discussed in more detail in the following. Since the physical CTS's frequency is obtained from the master clock with periodic frequency steering, the frequency adjustment quantity is constant during an adjustment interval. When the averaging time is shorter than the adjustment interval, the fluctuation of the fractional frequency difference introduced by frequency steering is smaller compared with that caused by the noise of the master clock. This explains why physical CTS's SSSAI almost follows that of the master clock.

Generally, the stability of physical CTS is always inferior to that of paper CTS when the averaging time is around the adjustment interval.[24] It is reasonable because the periodic frequency steering is a periodic perturbation in frequency that will result in deterioration in stability when the averaging time is around the adjustment interval.

When the averaging time is longer than the adjustment interval, the effect of frequency steering appears. The adjustment is an open-loop control process based on the signal-based open-loop control approach.[25] At time epoch t, once $x_{\rm cr}(t)$, i.e., the paper CTS, the phase time difference between the CTS and the master clock, is derived, the phase time difference of the CTS with respect to an ideal clock, marked as $x_{\rm c}(t)$, can be expressed as

$$x_{\rm c}(t)=x_{\rm cr}(t)+x_{\rm r}(t). \tag{2}$$

Here, $x_{\rm r}(t)$ is the phase time difference of the master clock with respect to an ideal clock. The phase time difference of the CTS with respect to an ideal clock at time epoch $t+T$, $x_{\rm c}(t+T)$ can be calculated in a similar way. T is the calculation interval of the CTS. Then, the theoretical fractional frequency difference of the physical CTS against an ideal clock during the period from t to $t+T$, $y_c^{\rm theor}(t)$ can be calculated using the following equation:

$$\begin{aligned} y_{\rm c}^{\rm theor}(t)&=\frac{x_{\rm c}(t+T)-x_{\rm c}(t)}{T}\\ &=\frac{x_{\rm cr}(t+T)-x_{\rm cr}(t)}{T}+\frac{x_{\rm r}(t+T)-x_{\rm r}(t)}{T}\\ &=y_{\rm cr}^{\rm theor}(t)+y_{\rm r}(t), \end{aligned} \tag{3}$$

where $y_{\rm cr}^{\rm theor}(t)$ represents the theoretical fractional frequency difference of the CTS against the master clock, namely, the theoretical frequency adjustment quantity; $y_{\rm r}(t)$ represents the fractional frequency difference of the master clock against an ideal clock. Since $x_{\rm cr}(t+T)$ is not produced at time epoch t, $y_{\rm cr}^{\rm theor}(t)$ cannot be acquired at this epoch. However, frequency steering must be performed at time epoch t. Hence, it is of common practice to use a predicted adjustment quantity based on the theoretical frequency adjustment quantity of the last calculation interval as a substitute for frequency steering during this adjustment interval. The predicted frequency adjustment quantity, $y_{\rm cr}^{\rm pre}(t)$, can be calculated by

$$y_{\rm cr}^{\rm pre}(t)=y_{\rm cr}^{\rm theor}(t-T)+d_{\rm cr}\cdot T, \tag{4}$$

where $y_{\rm cr}^{\rm theor}(t-T)$ is the theoretical frequency adjustment quantity of the last calculation interval, and $d_{\rm cr}$ is the frequency drift of the CTS against the master clock. In the above equation, the change in fractional frequency difference caused by frequency drift can be estimated by

$$\begin{aligned} \Delta y_{\rm d}(t)&=d_{\rm cr}\cdot T\sim10^{-21}\cdot10^{3}\\ &=10^{-18}\ll y_{\rm cr}^{\rm theor}(t-T)\sim10^{-15}. \end{aligned} \tag{5}$$

It is three orders of magnitude smaller than $y_{\rm cr}^{\rm theor}(t-T)$, which is generally on the order of 10^{-15} and can be neglected. Therefore, we take the fractional frequency difference $y_{\rm cr}^{\rm theor}(t-T)$ to adjust the frequency of the AOG during the period from t to $t+T$. In this way, the practical fractional frequency difference of the physical CTS with respect to an ideal clock, $y_{\rm c}^{\rm prac}(t)$, can be formulated as

$$y_{\rm c}^{\rm prac}(t)=y_{\rm cr}^{\rm theor}(t-T)+y_{\rm r}(t). \tag{6}$$

The frequency error between the theoretical fractional frequency difference and the practical fractional frequency difference of the physical CTS, $\Delta y_{\rm c}(t)$, can be estimated by

$$\begin{aligned} \Delta y_{\rm c}(t)&=y_{\rm c}^{\rm theor}(t)-y_{\rm c}^{\rm prac}(t)\\ &=y_{\rm cr}^{\rm theor}(t)-y_{\rm cr}^{\rm theor}(t-T)\sim\sigma_{\rm cr}(T)\approx\sigma_{\rm r}(T), \end{aligned} \tag{7}$$

where $\sigma_{\rm cr}(T)$ represents the relative stability of the paper CTS against the master clock, and $\sigma_{\rm r}(T)$ represents the individual stability of the master clock.

The magnitude of the frequency error is positively related to the relative stability of the paper CTS against the reference clock when the averaging time is equal to the adjustment interval. Furthermore, it is primarily dominated by the stability of the master clock. This also indicates that when the master clock is less stable, the frequency error will be larger. This frequency error will appear as the bias between the individual stability of paper CTS and that of physical CTS when the averaging time is longer than the adjustment interval until the region dominated by the frequency drift of the H-maser (averaging time longer than $\sim 10^5$ s). As shown in Fig. 2(d), when the averaging time is equal to the adjustment interval of 1200 s, the relative stability of the paper CTS against clock C is $\sim 1\times10^{-15}$, while the relative stability of the paper CTS against clock D is $\sim 3\times10^{-15}$. The relative stabilities of the paper CTSs with different reference clocks conform to the bias between the individual stabilities of paper CTSs and those of physical CTSs, as shown in Fig. 2(c).

The Allan variance of the practical physical CTS, $\sigma_{\rm c}^2(\tau)$, can be further derived as

$$\begin{aligned}\sigma_{\rm c}^2(\tau) &= \frac{1}{2}\langle(y_{\rm c}^{\rm prac}(t)-y_{\rm c}^{\rm prac}(t-\tau))^2\rangle = \frac{1}{2}\langle(\Delta y_{\rm c}^{\rm prac}(t))^2\rangle\\ &= \frac{1}{2}\langle(\Delta y_{\rm cr}^{\rm theor}(t-T)+\Delta y_{\rm r}(t))^2\rangle\\ &= \frac{1}{2}\langle(\Delta y_{\rm cr}^{\rm theor}(t-T))^2+(\Delta y_{\rm r}(t))^2\\ &\quad +2\cdot\Delta y_{\rm cr}^{\rm theor}(t-T)\cdot\Delta y_{\rm r}(t)\rangle\\ &= \sigma_{\rm cr}^2(\tau)+\sigma_{\rm r}^2(\tau)+2{\rm Cov}_{{\rm cr}(t-\tau),r(t)}(\tau),\end{aligned} \tag{8}$$

where ${\rm Cov}_{{\rm cr}(t-\tau),r(t)}(\tau)$ is the Allan covariance calculated with the fractional frequency difference of the master clock $y_{\rm r}(t)$ and the theoretical frequency adjustment quantity of the last calculation interval $y_{\rm cr}^{\rm theor}(t-\tau)$; τ is the averaging time. For $y_{\rm r}(t)$ and $y_{\rm cr}^{\rm theor}(t)$, they are strictly negatively correlated; therefore, their Allan covariance (theoretical Allan covariance) is negative. It is exactly by virtue of this relationship that the CTS achieves better stability. However, due to the frequency error between $y_{\rm cr}^{\rm theor}(t)$ and $y_{\rm cr}^{\rm theor}(t-T)$, $y_{\rm r}(t)$ and $y_{\rm cr}^{\rm theor}(t-T)$ are no longer strictly negatively correlated with all averaging time. Furthermore, the less stable the master clock is, the larger the frequency error is, which in turn leads to a larger bias between their covariance and the theoretical covariance.

In conclusion, as a result of the frequency error introduced by open-loop steering with a deferred frequency adjustment quantity, the stability of the physical CTS is dependent strongly on that of the master clock, even with a large averaging time longer than the adjustment interval. This also proves the necessity of improving the performance of the physical CTS through the proposed scheme.

3. A real-time physical CTS referenced by the most stable clock based on a real-time clock network

As the stability of the physical CTS depends on that of the master clock, its stability will be further improved if the physical CTS can be realized based on an arbitrary clock with superior performance in the clock network. Meanwhile, generating excellent physical CTS is an essential ability for timekeeping institutions. If institutions are equipped with a superior master clock, there is no doubt that they will have an equal base to conduct timekeeping. For the entire clock network, it is possible to realize polycentric democratic timekeeping.

Inspired by this idea, a real-time clock network is depicted in Fig. 3(a). The network is supported by the fiber-based frequency synchronization technique introduced in Refs. [16, 26]. The frequency synchronization system used in the network can realize a frequency transfer stability of better than 1×10^{-14}/s and $1\times10^{-17}/10^5$ s, which is at least one order of magnitude better than that of the H-maser. This stability is sufficient to ensure the real-time transmission and recovery of the atomic clock signal at remote sites with no deterioration. Employing a few of frequency synchronization systems, H-masers located at different institutions are all connected. Local atomic clock and recovered remote atomic clock signals can be compared and measured simultaneously by a phase comparator at any institution.

Before the generation of physical CTS, the stability performance of each atomic clock needs to be calculated and analyzed based on collected phase time difference data. Utilizing individual stability estimation methods, such as the three-cornered-hat and N-cornered-hat methods described in Refs. [27,28], we can efficiently obtain the individual stability of each clock and determine the most stable clock. This clock is chosen to be the master clock of the clock ensemble.

At any institution, the CTS generation system consists of a phase comparator, an AOG and a computer. The phase time difference data are sent to a computer to calculate the paper CTS periodically and iteratively. Then, the computer controls an AOG referenced by the master clock to generate a real-time physical CTS with the best stability in the network. In this way, each institution will have the ability to build up the best physical CTS no matter whether it has the most stable clock.

Actually, the above network is redundant in devices. A compact real-time clock network is shown in Fig. 3(b). Under the premise of ensuring the stability and reliability of the CTS, institutions in the network can share phase difference data. In other words, a phase comparator placed at any institution in the network or even outside the network is enough to support the signal comparison task of the entire network, except that it needs to broadcast measured phase time difference data in a public way in real time, e.g., via the internet. The other institu-

tions in the network can download the data, and then the real-time CTS can be generated. Another option is to select one of the institutions as the paper CTS's generation center, where the paper CTS data with the master clock set as the reference are generated and broadcast. The other institution in the network can generate the best physical CTS by simply adjusting the frequency of the AOG referenced by the master clock signal at hand according to the broadcast paper CTS data. At the same time, it is unnecessary to transfer all the signals from remote atomic clocks to the local site for recovery. Once the master clock is determined, only the master clock signal needs to be distributed to each institution. In this way, apart from those institutions where the phase comparator and master clock are located, most institutions require only one transmitter and one receiver of the frequency synchronization system to transfer the local clock signal and receive the master clock signal.

Considering the practical distribution of the clock ensemble, the real-time clock network used in our experiment is shown in Fig. 3(c). Two sets of CTS generation systems are built at Tsinghua University. They share a common clock ensemble consisting of four H-masers from four institutions which are connected by fiber network. The length of fiber links is 39 km between H_3 and H_1, 21 km between H_3 and H_2, and 26 km between H_3 and H_4, respectively. The atomic clocks of different institutions are all placed in separate temperature-controlled chambers. The clock signals are compared at Tsinghua University, and phase time difference data are collected once a second. The calculation and adjustment interval of the CTS generation systems are both set to 1200 s. Through comparison, it is found that remote clock H_1 has the highest stability, while local clock H_3 has the lowest stability. To test the strength of the real-time network in practice, one of the physical CTSs is referenced by remote clock H_1. In contrast, the other physical CTS is referenced by local clock H_3. The algorithm used to calculate CTSs is AT1.

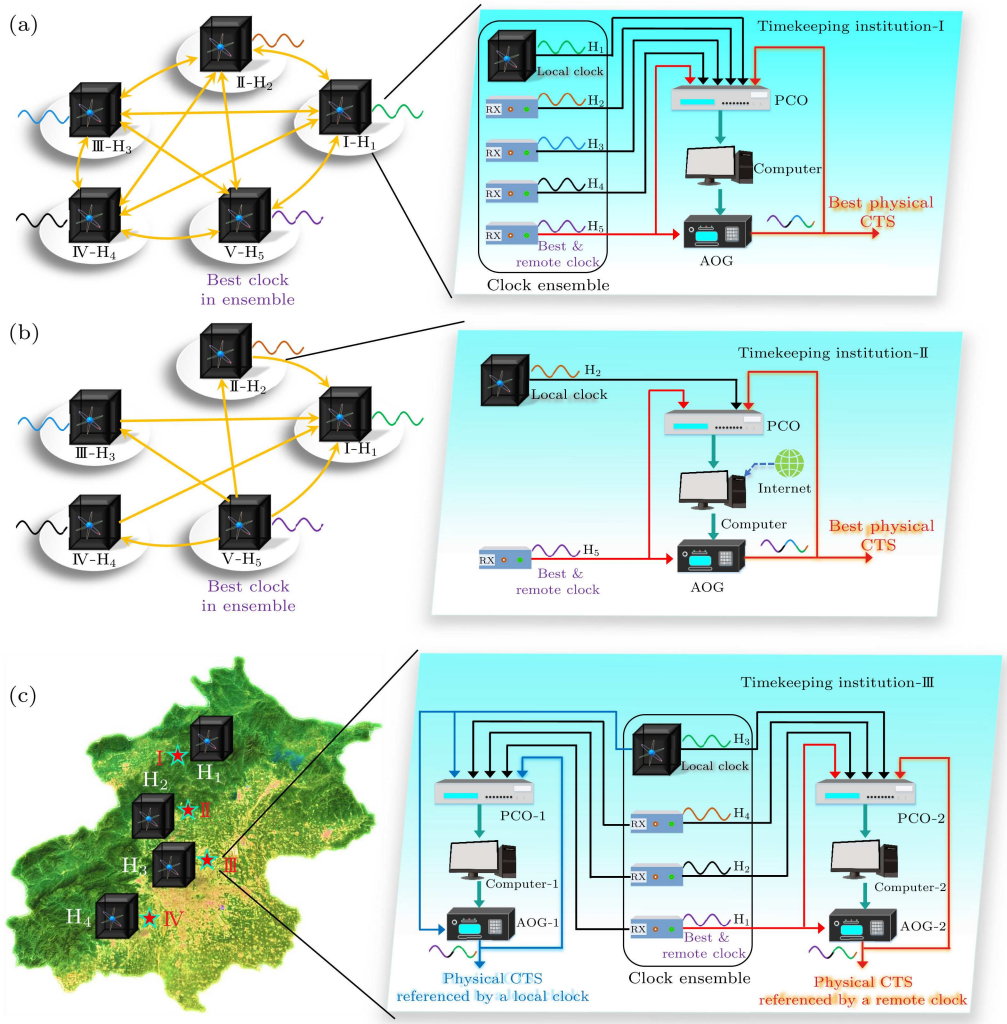


Fig. 3. (a) Schematic diagram of the real-time clock network with redundant devices; Ⅰ, Ⅱ, Ⅲ, Ⅳ, and Ⅴ: different institutions in the network; H_1, H_2, H_3, H_4, and H_5: H-masers from different institutions, and H_5 is the most stable clock in the clock ensemble; PCO: phase comparator; AOG: auxiliary output generator; CTS: composite time scale. (b) Schematic diagram of the compact real-time clock network. (c) Schematic diagram of the validation experiment for the real-time clock network, where two physical CTSs referenced by a less stable local clock and a stable remote clock respectively are built; Ⅰ, Ⅱ, Ⅲ, and Ⅳ: different institutions in Beijing, of which Ⅲ is Tsinghua University; H_1, H_2, H_3 and H_4: H-masers from different institutions, of which H_1 is the most stable clock in ensemble, and H_3 is the least stable clock in ensemble.

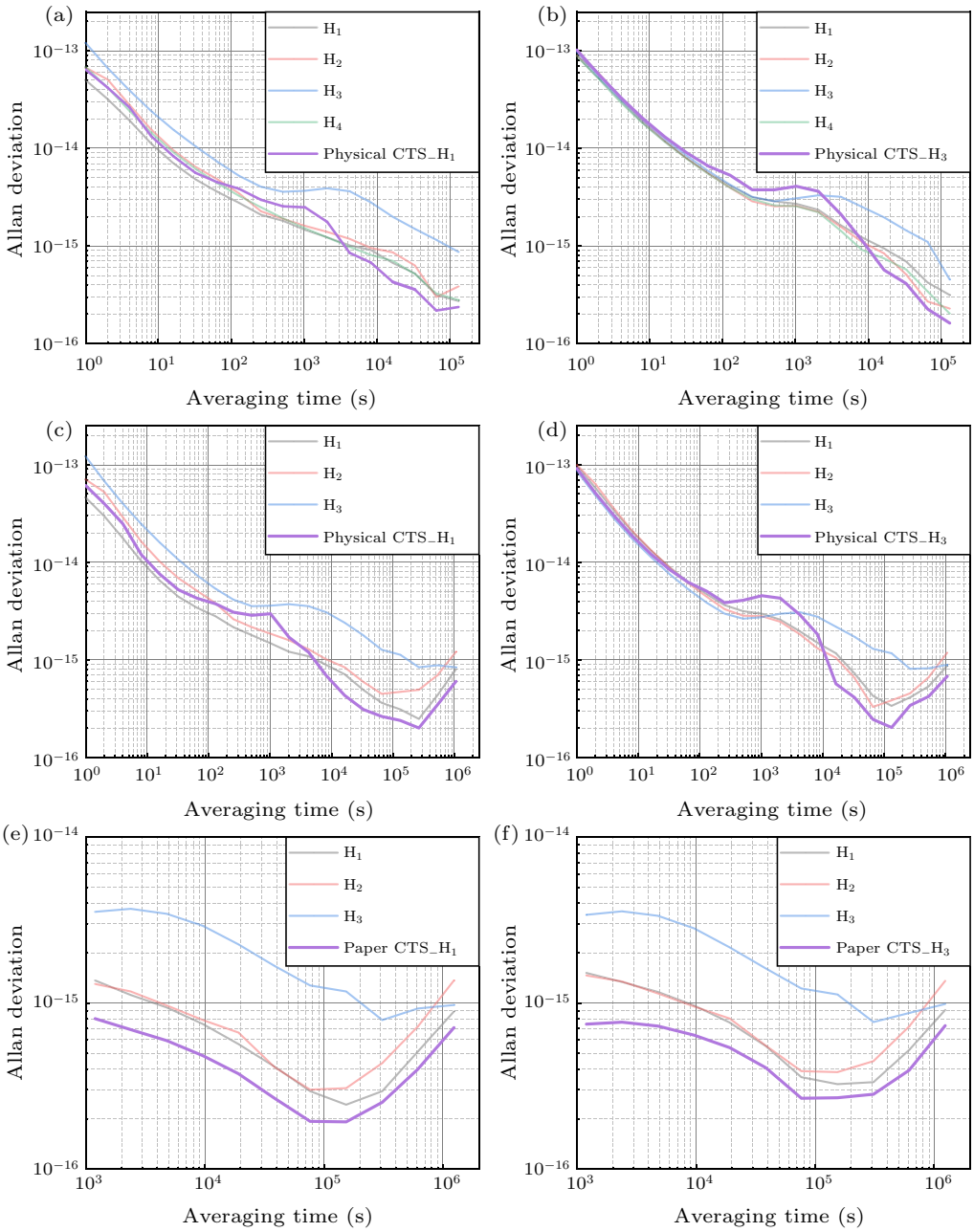


Fig. 4. Individual frequency stabilities calculated with the N-Cornered-Hat method. (a) Individual stability curves of physical CTSs referenced by H_1 (stable remote clock) and that of member clocks during the period (previous 15 days) when all four H-masers are present. H_1, H_2, H_3 and H_4: H-masers from different institutions. Physical CTS_H_1 represents physical CTS referenced by clock H_1, other legends have similar meanings. (b) Individual stability curves of physical CTSs referenced by H_3 (less stable local clock) and that of member clocks during the period (previous 15 days) when all four H-masers are present. (c) Individual stability curves of physical CTSs referenced by H_1 and that of member clocks (H_4 is not included because it is lost since the 16th day) throughout the experiment period (90 days). (d) Individual stability curves of physical CTSs referenced by H_3 and that of member clocks throughout the experiment period (90 days). (e) Individual stability curves of paper CTSs referenced by H_1 and that of member clocks throughout the experiment period (90 days). Paper CTS_H_1 represents paper CTS referenced by clock H_1, other legends have similar meanings. (d) Individual stability curves of paper CTSs referenced by H_3 and that of member clocks throughout the experiment period (90 days).

A continuous test of physical CTSs lasting 90 days is carried out. The results based on real measured data are shown in Fig. 4. Figures 4(a) and 4(b) reveal the individual stabilities of the two physical CTSs and those of the member clocks during the period (previous 15 days) when all four H-masers are present. The SSSAIs of the two physical CTSs almost follow that of their master clock. The physical CTS referenced by the most stable remote clock H_1 outperforms all member clocks when the averaging time is longer than ~ 4000 s. For the physical CTS referenced by the least stable local clock H_3, this time increases to ~ 10000 s. It is obvious that the stability of the physical CTS is improved when the stable remote clock is chosen to be the master clock with the help of the real-time clock network. Figures 4(c) and 4(d) show the individual stabilities of two physical CTSs and those of member clocks (H_4 is not included because it is lost since the 16th day) throughout

the experiment period (90 days). Compared with the results shown in Figs. 4(a) and 4(b) during the previous 15 days, the results containing data when H_4 is lost are not significantly deteriorated. Figures 4(e) and 4(f) show the individual stabilities of two paper CTSs and those of member clocks throughout the experiment period (90 days). The two paper CTSs outperform all clocks when the averaging time is longer than the calculation interval of CTSs. Their stabilities remain similar. The experimental results are perfectly in agreement with the simulation results in Section 2.

As another method to assess CTS's performance, we also compare two physical CTSs with UTCr respectively. The results are listed in Tables 2 and 3. The stabilities of H_1, H_2, H_3 and two physical CTSs are calculated with experimental data throughout the experiment period (90 days). As H_4 is lost since the 16th day, the stability of H_4 is obtained from experimental data collected during the previous 15 days.

The results reveal that the stabilities of two physical CTSs are close to each other when the averaging time is longer than one day, which is also shown in Figs. 4(c) and 4(d). This phenomenon is due to the predominant influence of frequency drift on frequency stabilities within this range and the effect of the frequency error related with the master clock is obscured. The results prove that the physical CTS referenced by remote master clock performs within the expected range.

Table 2. Frequency stabilities of each clock (used to generate physical CTS_H_1) with respect to UTCr.

Clock	H_1	H_2	H_3	H_4	Physical CTS_H_1
ADEV@1d	3.66×10^{-15}	3.84×10^{-15}	4.19×10^{-15}	4.00×10^{-15}	3.75×10^{-15}
ADEV@2d	2.21×10^{-15}	2.27×10^{-15}	3.07×10^{-15}	1.67×10^{-15}	2.31×10^{-15}
ADEV@4d	1.60×10^{-15}	1.73×10^{-15}	1.88×10^{-15}		1.63×10^{-15}
ADEV@8d	9.05×10^{-16}	1.36×10^{-15}	1.74×10^{-15}		1.06×10^{-15}

Table 3. Frequency stabilities of each clock (used to generate physical CTS_H_3) with respect to UTCr.

Clock	H_1	H_2	H_3	H_4	Physical CTS_H_3
ADEV@1d	3.66×10^{-15}	3.88×10^{-15}	4.00×10^{-15}	3.97×10^{-15}	3.72×10^{-15}
ADEV@2d	2.21×10^{-15}	2.30×10^{-15}	2.02×10^{-15}	1.60×10^{-15}	2.27×10^{-15}
ADEV@4d	1.60×10^{-15}	1.90×10^{-15}	1.52×10^{-15}		1.71×10^{-15}
ADEV@8d	9.05×10^{-16}	1.39×10^{-15}	1.37×10^{-15}		1.29×10^{-15}

4. Conclusion and discussion

In this paper, aiming at the adverse effects of the centralized timekeeping topology on conventional CTS, the stability limitation of the physical CTS caused by the selection of the master clock is simulated. The results prove that the LSLAI of the physical CTS is positively related to that of the master clock until the region dominated by the frequency drift of the H-maser (averaging time longer than $\sim 10^5$ s). Furthermore, the mechanism inherent in this limitation is given in detail, and we employ a real-time clock network to break the limitation. On this basis, a real-time physical CTS referenced by a stable remote master is achieved experimentally. The comparison experiment, where another physical CTS referenced by a less stable local master clock is generated simultaneously, shows that the stability of the physical CTS is obviously improved when the stable remote clock is chosen as the master clock. Compared with conventional physical CTSs, the proposed scheme enables real-time physical CTSs to be realized based on the most stable clock in the network, and the best physical CTS to be realized no matter whether the timekeeping institution has the most stable clock. The work is a key step to achieve the decentralized real-time timekeeping network on which the master clock can be switched among some stable clocks to further enhance the stability and reliability of the physical CTS.

On the other hand, it is worth noting that the proposed scheme still faces some challenges in its long-term operation, such as fiber link outages and uncompensated disturbances introduced by high-frequency vibrations during atomic clock signal transmission. We have designed a disturbance-resistant algorithm, described in Ref. [16], to cope with the above-mentioned disturbance and to ensure that the physical CTS operates smoothly, regardless of fiber link disturbances or ensemble member changes.

Acknowledgments

The authors would like to thank Dr. Yuzhuo Wang in National Institute of Metrology, China for providing UTCr comparison data, facilitating the evaluation of the physical CTSs' performance.

This work was supported in part by the National Natural Science Foundation of China (Grant No. 61971259), the National Key R&D Program of China (Grant No. 2021YFA1402102), and Tsinghua University Initiative Scientific Research Program.

References

[1] Yang Y X, Mao Y and Sun B J 2020 *Satell. Navig.* **1** 1

[2] Lévesque M and Tipper D 2016 *IEEE Commun. Surv. Tutor.* **18** 2926

[3] McGrew W F, Zhang X, Fasano R J, Schaffer S A, Beloy K, Nicolodi D, Brown R C, Hinkley N, Milani G, Schioppo M, Yoon T H and Ludlow A D 2018 *Nature* **564** 87

[4] Zhang Z H, Gong S P, Dimitrovski A D and Li H S 2013 *IEEE Trans. Smart Grid* **4** 87

[5] Kolkowitz S, Pikovski I, Langellier N, Lukin M D, Walsworth, R L and Ye J 2016 *Phys. Rev. D* **94** 124043

[6] Derevianko A and Pospelov M 2014 *Nat. Phys.* **10** 933

[7] Galleani L and Tavella P 2010 *IEEE Control Syst. Mag.* **30** 44

[8] Tavella P and Thomas C 1991 *Metrologia* **28** 57

[9] Panfilo G and Arias F 2019 *Metrologia* **56** 042001

[10] Parker T E and Levine J 1997 *IEEE Trans. Ultrason. Ferroelectr. Freq. Control* **44** 1239

[11] Matsakis D 2005 *Proceeding of IEEE International Frequency Control Symposium and Exposition*, August 29–31, Vancouver, Canada, p. 217

[12] Ido T, Fujieda M, Hachisu H, Hayasaka K, Kajita M, Kumagai M, Li Y, Matsubara K, Nagano S, Ohtsubo N, Hanado Y and Hosokawa M 2017 *The Science of Time 2016: Time in Astronomy & Society, Past, Present and Future* (Cham: Springer) p. 151

[13] Zhang A M, Gao Y, Liang K, Wang W B, Yang Z Q, Ning D Y and Fang Z J 2013 *Joint European Frequency and Time Forum & International Frequency Control Symposium*, July 21–25, Prague, Czech Republic, p. 654

[14] Shemar S L, Davis J A and Whibberley P B 2010 *EFTF-2010 24th European Frequency and Time Forum*, April 13–16, Noordwijk, Netherlands, p. 1

[15] Dong S W 2003 *Metrologia* **40** S249

[16] Guo Y C, Wang B, Wang F M, Shi F F, Zhang A M, Zhu X, Yang J, Feng K M, Han C H, Li T C and Wang L J 2019 *Metrologia* **56** 045003

[17] Marszalec M, Lusawa M, Czubla A and Lewandowski W 2013 *Joint European Frequency and Time Forum & International Frequency Control Symposium*, July 21–25, Prague, Czech Republic, p. 805

[18] Azoubib J, Nawrocki J and Lewandowski W 2003 *Metrologia* **40** S245

[19] Tavella P 2008 *Metrologia* **45** S183

[20] Panfilo G and Tavella P 2008 *Metrologia* **45** S108

[21] Zucca C and Tavella P 2005 *IEEE Trans. Ultrason. Ferroelectr. Freq. Control* **52** 289

[22] Levine J 1999 *Rev. Sci. Instrum.* **70** 2567

[23] Levine J 2012 *Rev. Sci. Instrum.* **83** 021101

[24] Thomas C, Wolf P and Tavella P 1994 *Time Scales BIPM Monographie* **94** 1

[25] Farina M, Galleani L, Tavella P and Bittanti S 2010 *IEEE Trans. Ultrason. Ferroelectr. Freq. Control* **57** 2257

[26] Wang B, Gao C, Chen W L, Miao J, Zhu X, Bai Y, Zhang J W, Feng Y Y, Li T C and Wang L J 2012 *Sci. Rep.* **2** 556

[27] Tavella P and Premoli A 1994 *Metrologia* **30** 479

[28] Torcaso F, Ekstrom C R, Burt E A and Matsakis D N 2000 *IEEE Trans. Ultrason. Ferroelectr. Freq. Control* **47** 1183